Progress In Electromagnetics Research C, Vol. 115, 1–15, 2021

Hexagonal Split Ring Resonator Enclosed Circular Split Ring Resonator Inspired Dual-Band Antenna for Sub-6 GHz 5G NR and IEEE 802.11ba/be Applications

P. Rajalakshmi* and N. Gunavathi

Abstract—In this article, a novel Hexagonal Split-Ring Resonator enclosed Circular Split-Ring Resonator (HSRR-CSRR) inspired printed antenna is presented for sub-6 GHz 5G NR and IEEE 802.11ba/be applications. The proposed antenna comprises an HSRR-CSRR and a D-SHSRR metamaterial unit cell with a partial ground plane. The designed antenna is printed on a low-cost FR-4 substrate with dielectric constant ε_r of 4.4, thickness of 1.6 mm, and loss tangent of 0.02. An HSRR-CSRR metamaterial structure is designed to get the three distinct resonance frequencies at 3.5 GHz, 5.05 GHz, and 6.2 GHz, respectively. To cover the entire band of Sub-6 GHz 5G NR (5–6 GHz), a Double-slit Single Hexagonal Split Ring Resonator (D-SHSRR) is designed for 5.8 GHz and loaded along with the HSRR-CSRR. The operating principle, equivalent circuit, and parametric extraction of the HSRR-CSRR structure are examined. Compared to the conventional antenna, the proposed antenna has a compact size of $0.38\lambda_g \times 0.52\lambda_g \times 0.03\lambda_g$. The antenna parameters have been investigated using Ansys HFSS 15.0 software. The measured and simulated results are in good agreement.

1. INTRODUCTION

The International Telecommunication Union (ITU) has recently declared the following spectrum for 5G, including the 3.4–3.6 GHz, 5–6 GHz, 24.25–27.50 GHz, 37.0–40.5 GHz, and 66–76 GHz bands [1]. The IEEE 802.11 working group will release a new standard of 802.11 ba/be to improve the energy-efficient and extremely high throughput [2, 3]. Hence, there is a necessity to design a dual-band/wide-band antenna that is applicable to the upcoming IEEE standards (IEEE 802.11ba (2.4/5 GHz) and IEEE 802.11be (2.4/5/6 GHz)) and Sub-6 GHz 5G applications. Metamaterials are artificial materials that are not found in nature. They exhibit various properties such as negative permittivity, negative permeability, and negative refractive index. The use of metamaterials in antenna design reduces the size of the antenna and improves other antenna parameters such as bandwidth, gain, and number of frequency band [4, 5].

The CPW fed planar antennas [6–8], a spiral CSRR loaded antenna [9], and a circular SRR inspired antenna [10] are proposed for single-band operation. A hexagonal split-ring metamaterial-inspired dual-band antenna [11], a circular CSRR inspired cross-shaped dual-band antenna [12], and a triangular SRR metamaterial-inspired dual-band antenna [13] are designed for WLAN applications. An SRR inspired antenna [14], an electric LC loading based on Koch shaped fractal metamaterial antenna [15], a metamaterial slot inspired substrate waveguide antenna [16], a complementary capacitive-loaded loop antenna [17], a metamaterial with ELC and EBG loading antenna [18], a metamaterial inspired mushroom loaded antenna [19], a dumbbell shaped metamaterial inspired antenna [20], and a modified

Received 5 July 2021, Accepted 3 August 2021, Scheduled 13 August 2021

* Corresponding author: Pitchai Rajalakshmi (rajalakshmipitchai10@gmail.com).

The authors are with the Department of Electronics and Communication Engineering, National Institute of Technology, Tiruchirappalli, Tamilnadu 620015, India.

complementary hexagonal spiral resonator inspired antenna [21] have been realized for multiband performances, which are not focused on specific applications. A narrow-band single-loop resonator integrated monopole antenna is presented [22]. A low gain metamaterial-inspired antenna has been discussed in [23]. A complex profile and large dimension AMC reflector-based antenna has been proposed in [24]. For the miniaturization concept, a complex metamaterial-inspired RIS antenna has been developed in [25]. A complex 7×7 rectangular metasurface structure-based antenna has been designed for bandwidth enhancement [26]. An AMC integrated probe fed hexagonal ring antenna is presented for S-band applications with very low antenna efficiency of 45% [27]. A microstrip-fed hexagonal shape monopole antenna and a circular SRR-based monopole antenna have been designed for UWB band applications [28, 29]. A double negative circular CSRR antenna has been designed for 5G applications, which fails to cover the 3.4–3.6 GHz frequency band of sub 6GHz 5G applications [30].

All of the earlier researchers have examined concerns such as large size, single band, narrow bandwidth, and design complexity. However, it is unsuitable for upcoming 5G applications. To overcome all these challenges, this work has been investigated, analyzed, and validated. The proposed antenna employs HSRR-CSRR and D-SHSRR metamaterial structures to attain the required dual-band, size reduction, and bandwidth enhancement. These unique feature of the proposed antenna that is most suitable for the upcoming IEEE 802.11ba (2.4/5 GHz), IEEE 802.11be (2.4/5/6 GHz), and Sub-6 GHz (3.4–3.6 GHz and 5–6 GHz) 5G NR Wi-Fi applications.

2. ANTENNA STRUCTURE AND DESIGN METHODOLOGY

The evolutionary stages of the proposed antenna are illustrated in Figure 1. The final geometry of the proposed antenna is shown in Figure 2. It is implemented on a double-sided Printed Circuit Board (PCB) with FR4 substrate of permittivity (ε_r), thickness (h), and loss tangent δ of 4.4, 1.6 mm and 0.02, respectively, with a compact size of $20 \times 27 \times 1.6\,\text{mm}^3$. The antenna comprises a 50 Ω microstrip feed line, an HSRR-CSRR, a D-SHSRR on the top of the PCB, and a partial ground plane is entrenched on the bottom of the PCB.

Figure 1. Design of evolutionary stages of the proposed antenna. (a) Antenna 1. (b) Antenna 2. (c) Proposed antenna

Initially, the co-directional concentric HSRR is designed for 3.5 GHz. Hence, the length ($L_{3.5\,\text{GHz}}$) of the outer concentric hexagonal ring has taken as a half of the guided wavelength.

$$L_{3.5\,\text{GHz}} = \frac{c}{2f_r\sqrt{\varepsilon_{eff}}} = 26.1\,\text{mm} = 3S_1 \tag{1}$$

where c is the velocity of light in air; S_1 is the side of the outer hexagonal ring; ε_{eff} is the effective dielectric constant of the substrate.

In antenna 1, the outer concentric hexagonal split ring is connected to the inner concentric hexagonal split ring with the help of a metallic stub. The metallic stub's presence modifies the current distribution of the concentric HSRR and produces dual resonance mode at 3.57 GHz (TM_{10})

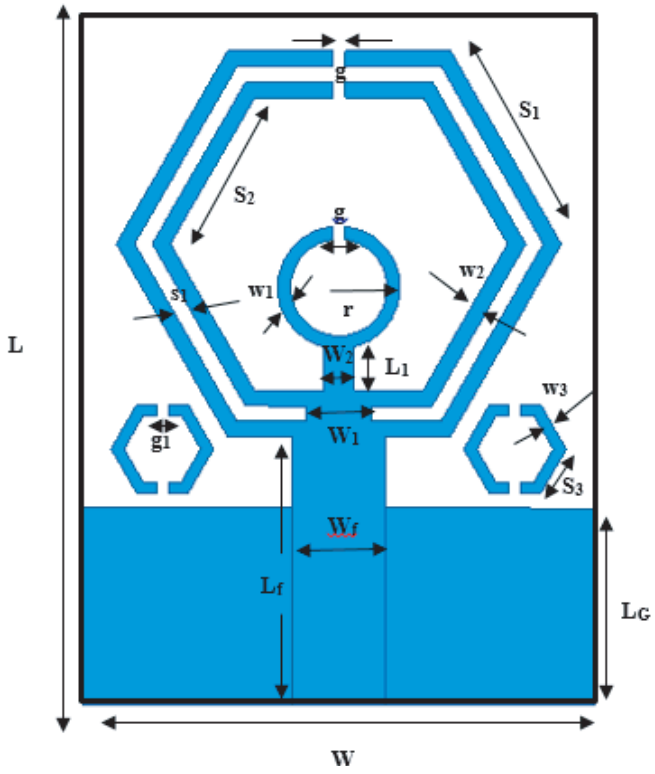

Figure 2. The geometry of the proposed antenna.

and 6.28 GHz (TM_{20}). The length ($L_{6.28\,GHz}$) of the concentric hexagonal ring is calculated using Equation (2). A single CSRR is designed for 5.3 GHz using the Equation (3)

$$L_{6.28\,GHz} = \frac{c}{4f_r\sqrt{\varepsilon_{eff}}} = 13.08\,mm \tag{2}$$

$$L_{5.3\,GHz} = \frac{c}{2f_r\sqrt{\varepsilon_{eff}}} = 2\pi r - g + L_1 = 17.3\,mm \tag{3}$$

where r and g are the radius and gap of the circular ring, respectively. Due to the coupling produced by the stub (L_1) with the single CSRR, antenna 2 has resonated at 3.47 GHz, 4.95 GHz, and 6.2 GHz to cover three different frequency bands 3.18–3.80 GHz, 4.80–5.20 GHz, and 6.07–6.23 GHz. Finally,

Table 1. Optimized dimensions of the proposed antenna.

Parameters	Dimensions (mm)	Parameters	Dimensions (mm)
L	27	W_1	2.6
W	20	W_2	1.2
L_G	7.7	S_1	8.7
L_f	10.5	S_2	6.6
W_f	3.6	S_3	2
s_1	0.7	L_1	2
R	2.4	w_3	0.5
w_2	0.7	g, g_1	0.5
w_1	0.5	h	1.6

the radiating element looks like an HSRR-CSRR metamaterial structure. Moreover, to cover the entire band of sub-6 GHz 5G NR (5–6 GHz), the two hexagonal split-ring resonators with two slits (D-SHSRR) are designed for 5.8 GHz. They are mounted on the top of the substrate as shown in Figure 1(c).

Based on the antenna's parametric study, the antenna's geometrical parameters are optimized and listed in Table 1. Also, the simulated reflection coefficient (in dB) of the proposed antenna is shown in Figure 3. From Figure 3, the proposed antenna resonates at 3.5 GHz, 5.07 GHz, and 6.1 GHz. Finally, the simulated 10 dB impedance bandwidth of the two operating bands are 15.88% (3.22–3.84 GHz) and 27.02% (4.80–6.30 GHz).

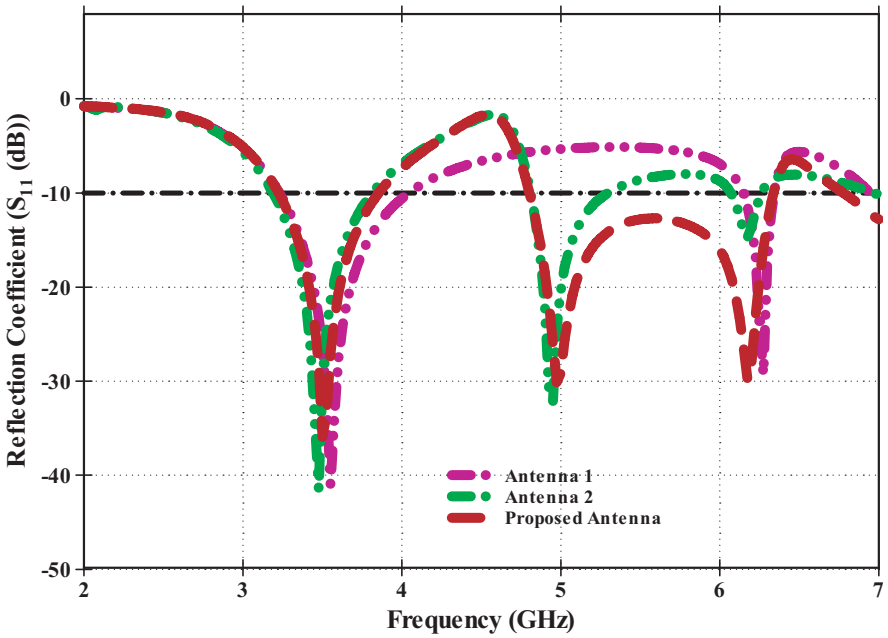

Figure 3. Simulated reflection coefficient (dB) characteristics of the evolutionary stages of antenna.

3. HSRR-CSRR METAMATERIAL STRUCTURE DESIGN METHODOLOGY

The HSRR-CSRR structure is derived from a concentric HSRR and a single CSRR connected via metallic stub. The dimension of the HSRR-CSRR is $20 \times 20\,\text{mm}^2$.

Figure 4 shows the equivalent circuit of the proposed HSRR-CSRR structure. The following equation is used to find out the resonance frequency of the LC circuit.

$$f_r = \frac{1}{2\pi\sqrt{L_{eq}C_{eq}}} \tag{4}$$

L_{eq} and C_{eq} are equivalent inductance and capacitance of the HSRR-CSRR structure. The following formulas are used to determine the L_{eq} and C_{eq} value of the structure [31].

$$L\,(\text{nH}) = 2 * 10^{-4} l \left[\ln\left(\frac{l}{w+t}\right) + 1.193 + 0.02235\frac{w+t}{l}\right] C_a \tag{5}$$

Here w, t, and l are the width, thickness, and length of the structure. The correction factor, C_a

$$C_a = 0.57 - 0.145\ln\left(\frac{w}{h}\right) \tag{6}$$

Here h and w represent the height and width of the substrate.

$$C = \frac{\varepsilon_0\varepsilon_r A}{d} \tag{7}$$

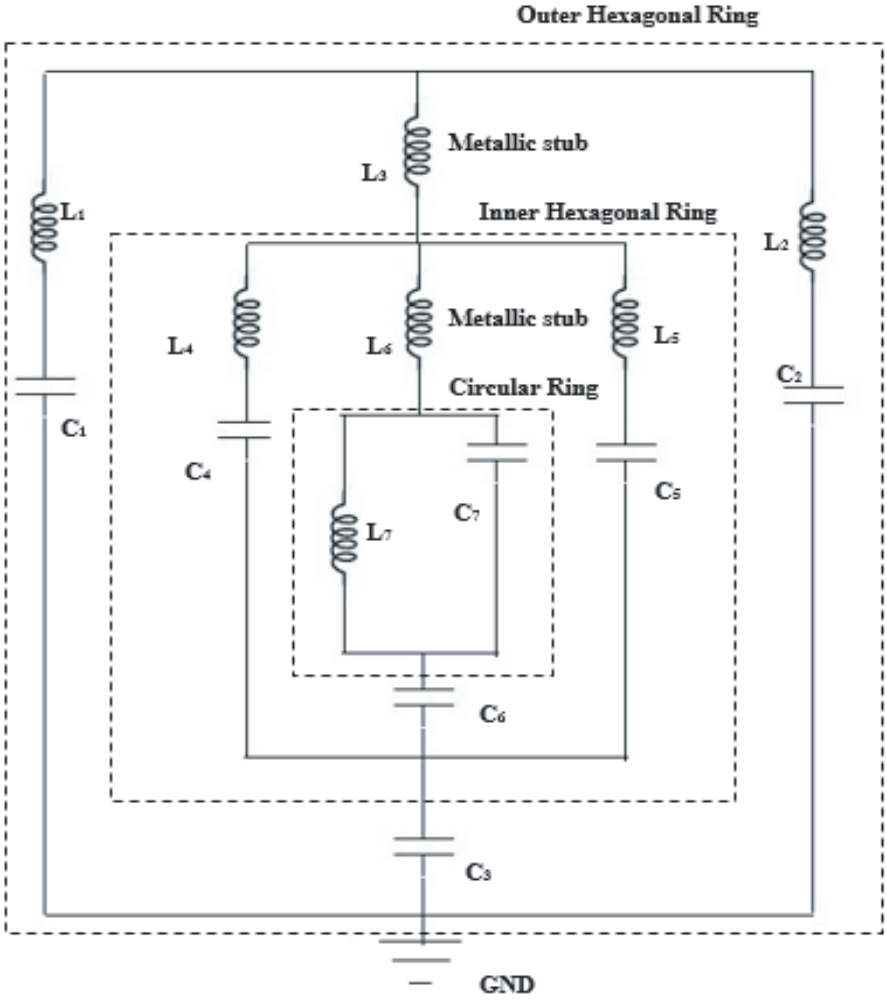

Figure 4. Equivalent circuit of the HSRR-CSRR metamaterial structure.

Here ε_0 and ε_r represent the free space of permittivity and relative permittivity of the dielectric substrate material. d and A represent the length of the split and the area of the structure.

The waveguide setup method was proposed by Chen et al. [32]. The wave guide setup of HSRR-CSRR structure is shown in Figure 5. By using the S_{11} and S_{21} generated with HFSS, the negative permeability of HSRR-CSRR is retrieved. The z (Characteristic impedance) and n (Refractive Index) are computed by Equations (8) and (9), respectively. In a waveguide setup, Perfect Electric Conductor (PEC) and Perfect Magnetic Conductor (PMC) boundary are assigned in y and z-direction, respectively. The electromagnetic wave is propagated in the z-direction.

$$z = \sqrt{\frac{(1+S_{11})^2 - S_{21}^2}{(1-S_{11})^2 - S_{21}^2}} \tag{8}$$

$$n = \frac{1}{kd}\cos^{-1}\left[\frac{1}{2S_{21}(1-S_{11}^2+S_{21}^2)}\right] \tag{9}$$

$$\varepsilon = \frac{n}{z} \tag{10}$$

$$\mu = nz \tag{11}$$

The negative permeability (μ) of the HSRR-CSRR metamaterial structure is calculated using the method suggested by Smith et al., which is given in Equation (11) [33]. The proposed metamaterial

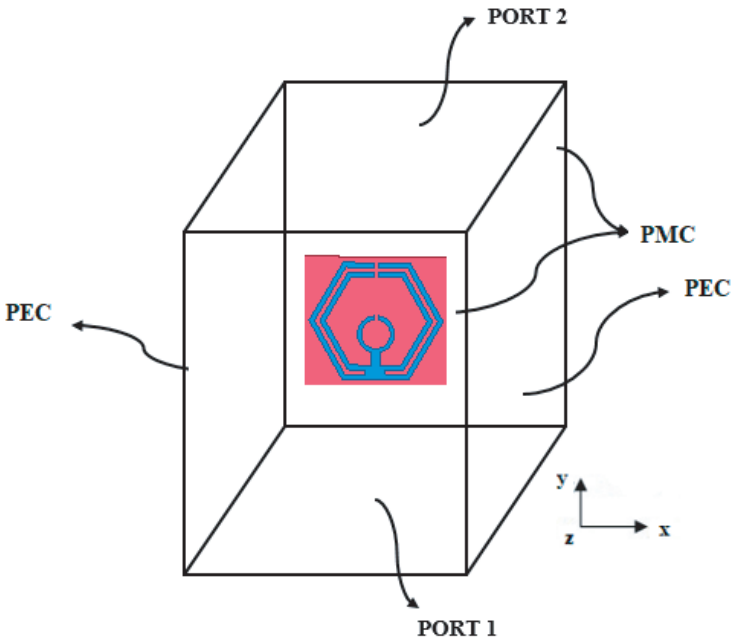

Figure 5. Simulation waveguide setup of the HSRR-CSRR metamaterial inspired structure.

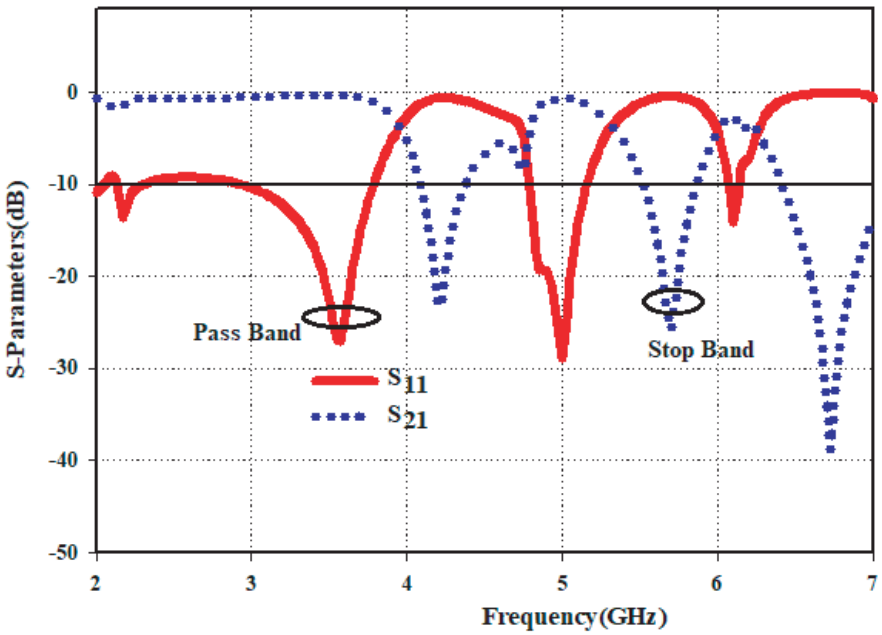

Figure 6. Transmission (S_{11}) and Reflection (S_{21}) characteristics of the HSRR-CSRR structure.

characteristics of the HSRR-CSRR structure are validated from its transmission, reflection, and permeability characteristics plots, as shown in Figure 6 and Figure 7. There are three negative permeability dips at 3.5 GHz, 5.2 GHz, and 6.15 GHz. The HSRR-CSRR structure's negative permeability property influenced the proposed antenna's performance parameters such as size reduction and multiband.

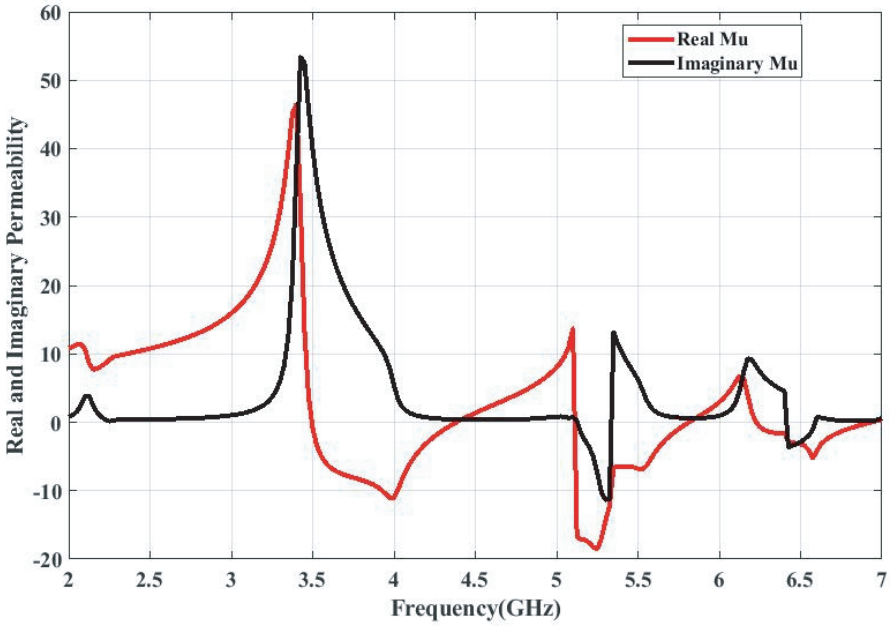

Figure 7. The negative permeability of the HSRR-CSRR metamaterial structure.

4. PARAMETRIC STUDIES

More impact parameters of the antenna such as ground length (L_G), hexagonal side length (S_1), feed width (W_f), and circular ring radius (r) are studied, and simulated reflection coefficient characteristics are plotted in Figures 8–11.

The effect of L_G on the antenna reflection coefficient (dB) characteristics is illustrated in Figure 8.

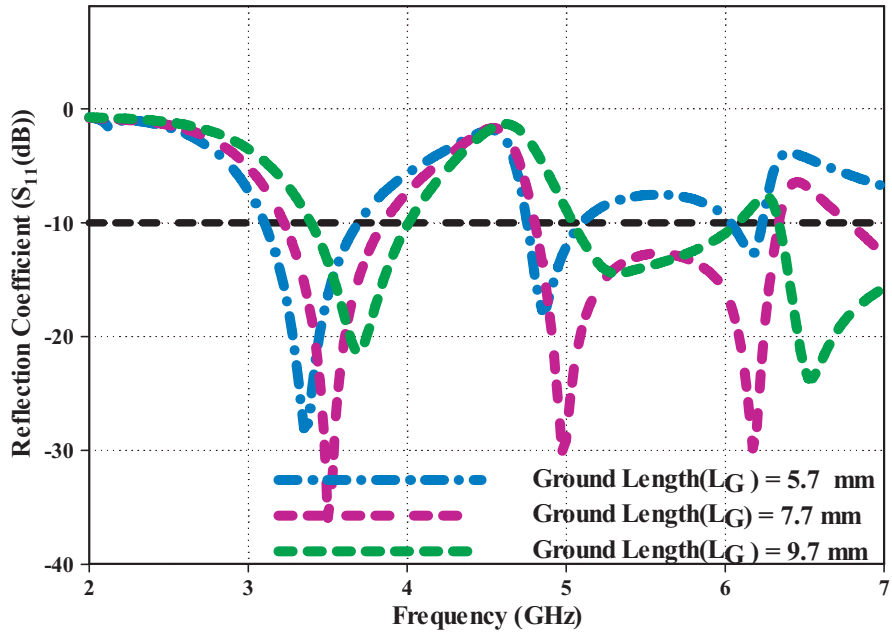

Figure 8. Simulated reflection coefficient characteristics (dB) of the variations of the ground length (L_G).

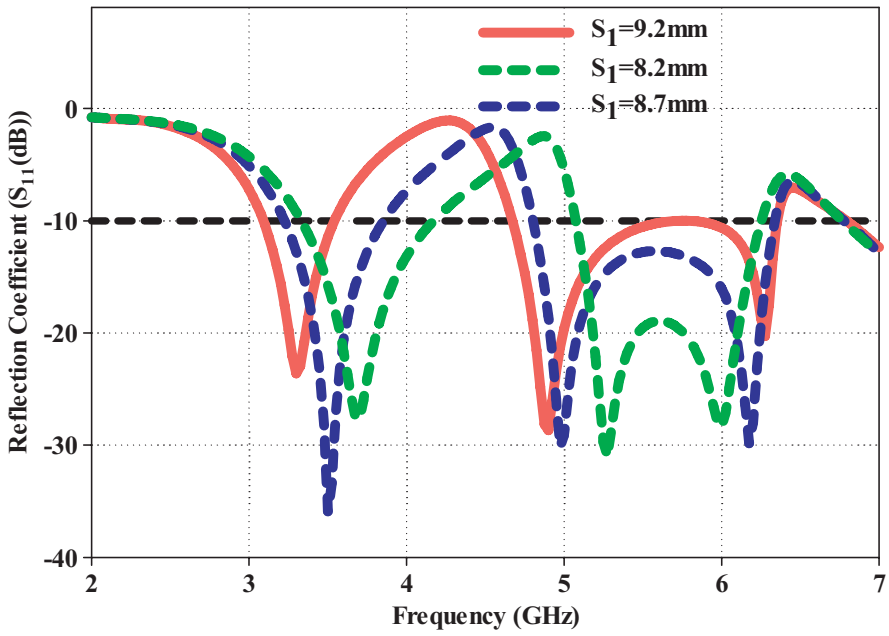

Figure 9. Simulated reflection coefficient characteristics (dB) of the variations of the hexagonal ring side length (S_1).

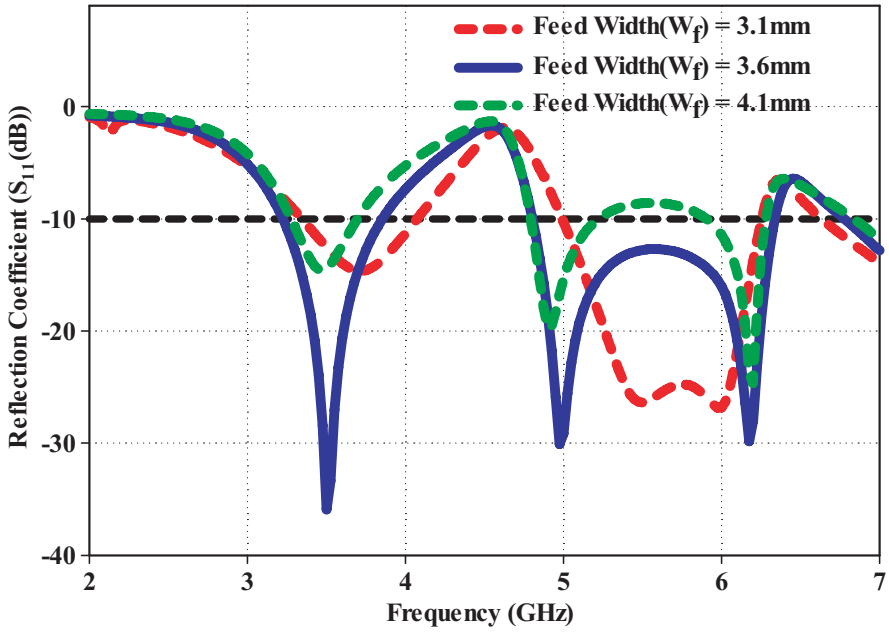

Figure 10. Simulated reflection coefficient characteristics (dB) of the variations of the feed width (W_f).

With the increasing value of L_G, the first resonance band of the proposed antenna is slightly increased, and also, the second resonance band is inflated with poor impedance matching. Preferred dual bands have been obtained at $L_G = 7.7$ mm. Figure 9 shows that by increasing S_1 from 8.2 mm to 9.2 mm with a step of 0.5 mm, the dual bands (TM_{10} and TM_{20}) are significantly affected. By decreasing the value of S_1, the first and second resonance frequencies of the antenna are increased. The $S_1 = 8.7$ mm is chosen from the results, covering the desired dual-band (3.22–3.84 GHz and 4.80–6.30 GHz) with good

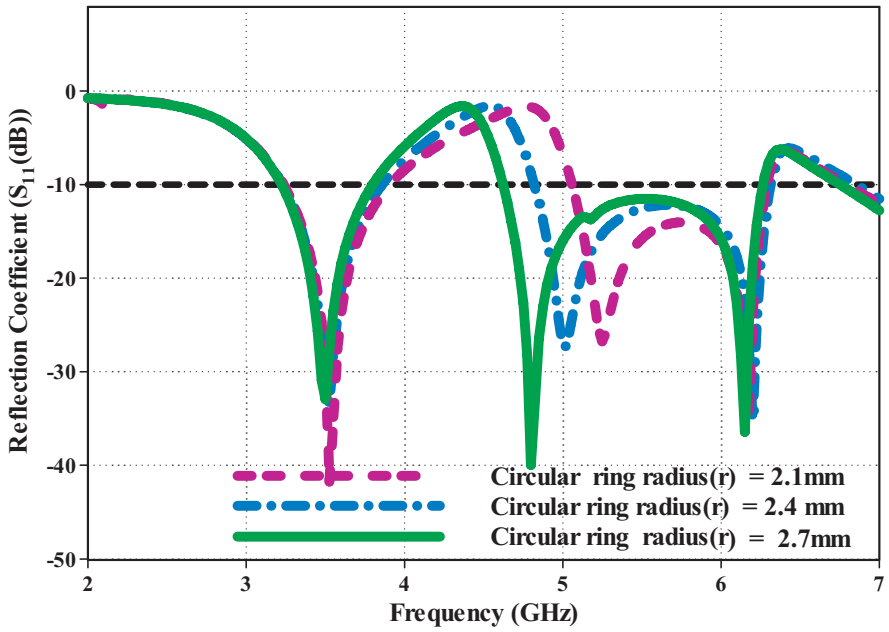

Figure 11. Simulated reflection coefficient (dB) characteristics of the variations of the circular ring radius (r).

impedance matching.

The reflection coefficient characteristics (dB) of various feed widths (W_f) of the proposed antenna from 3.1 mm with a step of 0.5 mm are shown in Figure 10. The impedance matching of the antenna is dependent on the W_f. The first band of 3.22–3.84 GHz and the second band of 4.80–6.30 GHz provide a good impedance matching at 3.6 mm. Figure 11 shows the effect of circular ring radius (r) on the antenna's reflection coefficient characteristics (dB). By increasing the circular ring radius (r) from 2.3 mm to 2.7 mm with a step of 0.2 mm, the resonant frequency of 5 GHz is shifted to lower frequencies. The desired resonance band is obtained at a circular ring radius (r) of 2.4 mm.

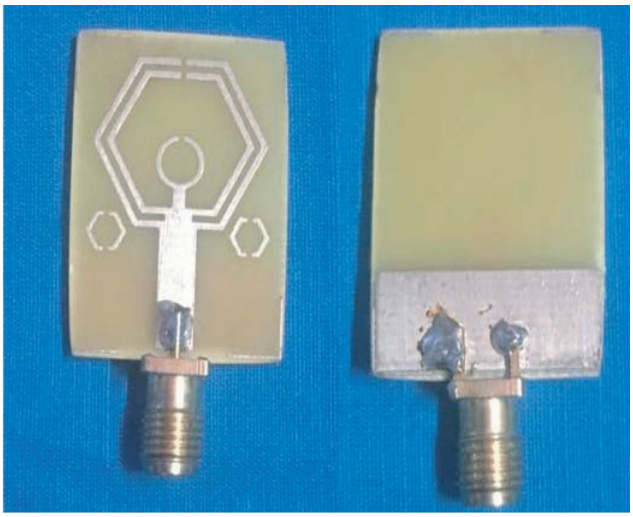

Figure 12. The fabricated proposed antenna.

5. RESULT AND DISCUSSION

The fabricated antenna is shown in Figure 12. The proposed antenna reflection coefficient (dB) has been measured with the help of vector keysight field fox microwave analyzer N99917A. The simulated and measured reflection coefficient results of the antenna are illustrated in Figure 13. It is observed that the simulated and measured reflections of the coefficient results are in good agreement, showing a dual-band operation with measured −10 dB impedance bandwidth of 625 MHz (3225–3850 MHz), 2030 MHz (4820–6850 MHz). The obtained bandwidth covers the upcoming Wi-Fi band (IEEE 802.11ba (2.4/5 GHz)/IEEE 802.11be (2.4/5/6 GHz)) and Sub-6 GHz 5G NR (3.4–3.6 GHz and 5–6 GHz) applications. The antenna's radiation efficiency is 97% at 3.5 GHz, 91.23% at 5.05 GHz, and 90.84% at 6.2 GHz, respectively. It is clearly noted that more than 90% of antenna efficiency has been obtained, which indicates that the antenna radiates well for the desired dual-band. The simulated gains of 3.5 GHz, 5.05 GHz, and 6.2 GHz are 1.78 dB, 1.83 dB and 2.3 dB, respectively.

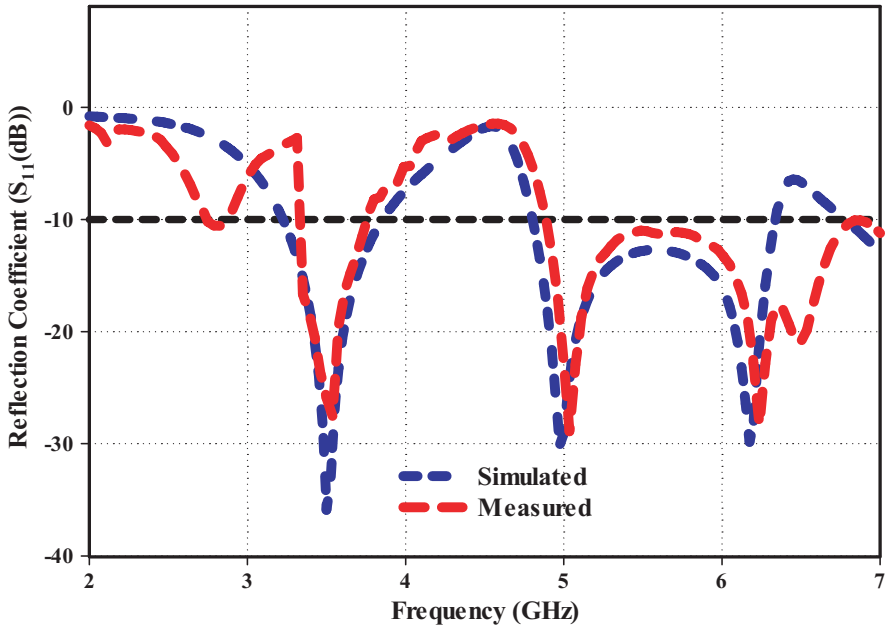

Figure 13. The simulated and measured reflection coefficient of the proposed antenna.

The simulated and measured radiation patterns on the x-z plane (E-plane) and x-y plane (H-plane) plane for 3.5 GHz, 5.05 GHz, and 6.20 GHz are shown in the Figures 14(a), (b), and (c), respectively. It shows that the proposed antenna exhibits an omnidirectional radiation pattern in the H-plane (x-y plane) at the proposed antenna's respective bands. The E-plane radiation pattern (x-z plane) is a dipole radiation pattern for all the proposed antenna operating bands.

The surface and vector current distribution of the HSRR-CSRR radiating element and the ground plane for various frequencies is simulated and presented in Figure 15. Figure 15(a) shows the current distribution at 3.52 GHz. It can be well noted that maximum current is distributed on the two concentric hexagonal rings and feed line. It can be concluded from Figure 15(a) that two concentric hexagonal rings are most important in adjusting the lower resonance frequency (3.52 GHz). Figure 15(b) represents the surface and vector current distribution on the antenna for 5.05 GHz. It can be noted that most of the current is concentrated on the inner circular ring only. In contrast, a marginal current is symmetrically distributed on the left/right side of the ring. Hence, the middle resonance frequency can be mainly controlled through the circular ring. Figure 15(c) shows the surface current on the HSRR-CSRR as well as on the ground for the resonant frequency of 6.2 GHz. It is obvious from Figure 15(c) that the major content of the current is concentrated on the upper and lower part of the two concentric hexagonal rings.It can be well noted from this figure that the third resonance frequency is controlled by changing

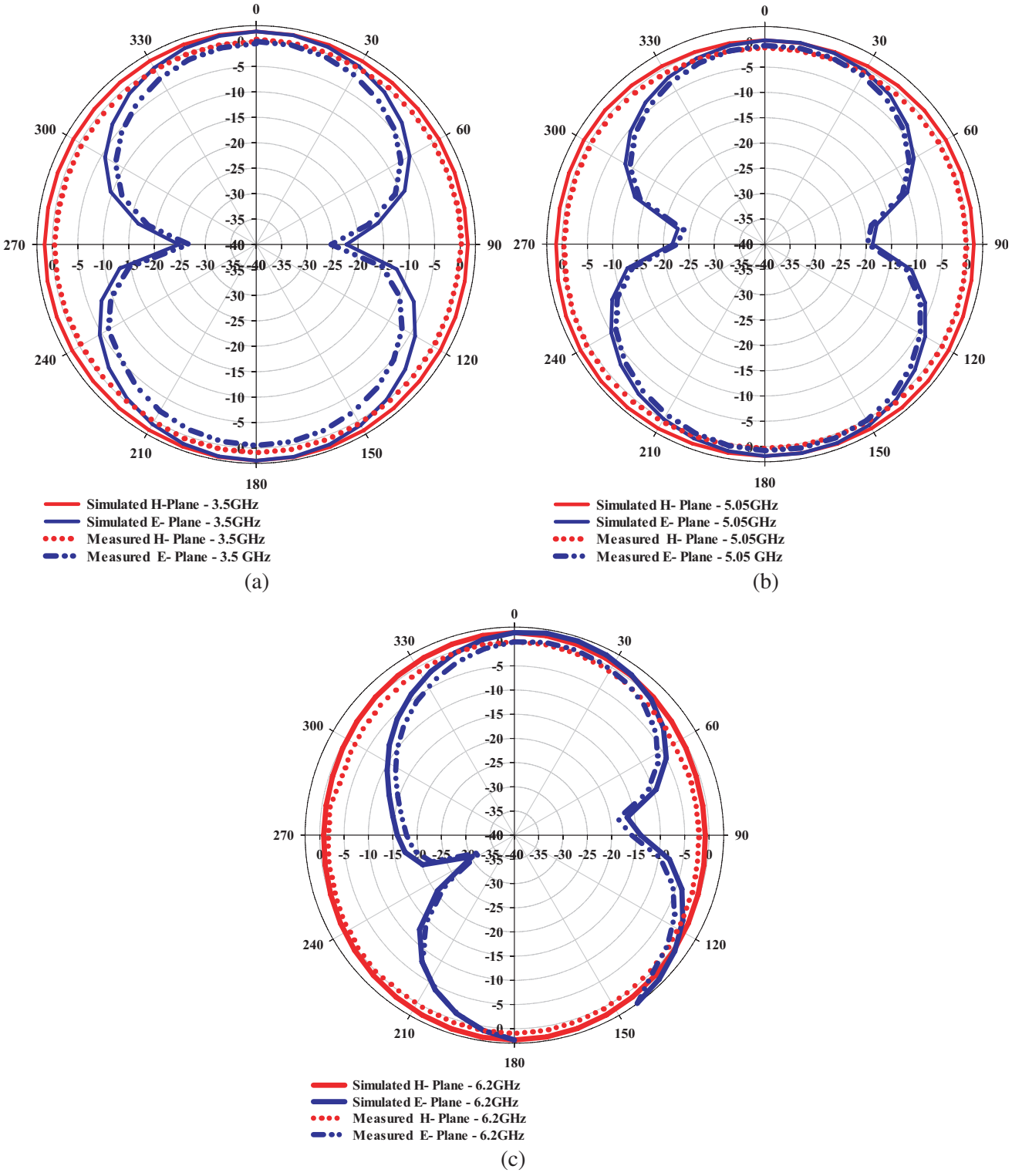

Figure 14. The simulated and measured radiation pattern of the proposed antenna. (a) 3.5 GHz. (b) 5.05 GHz. (c) 6.2 GHz.

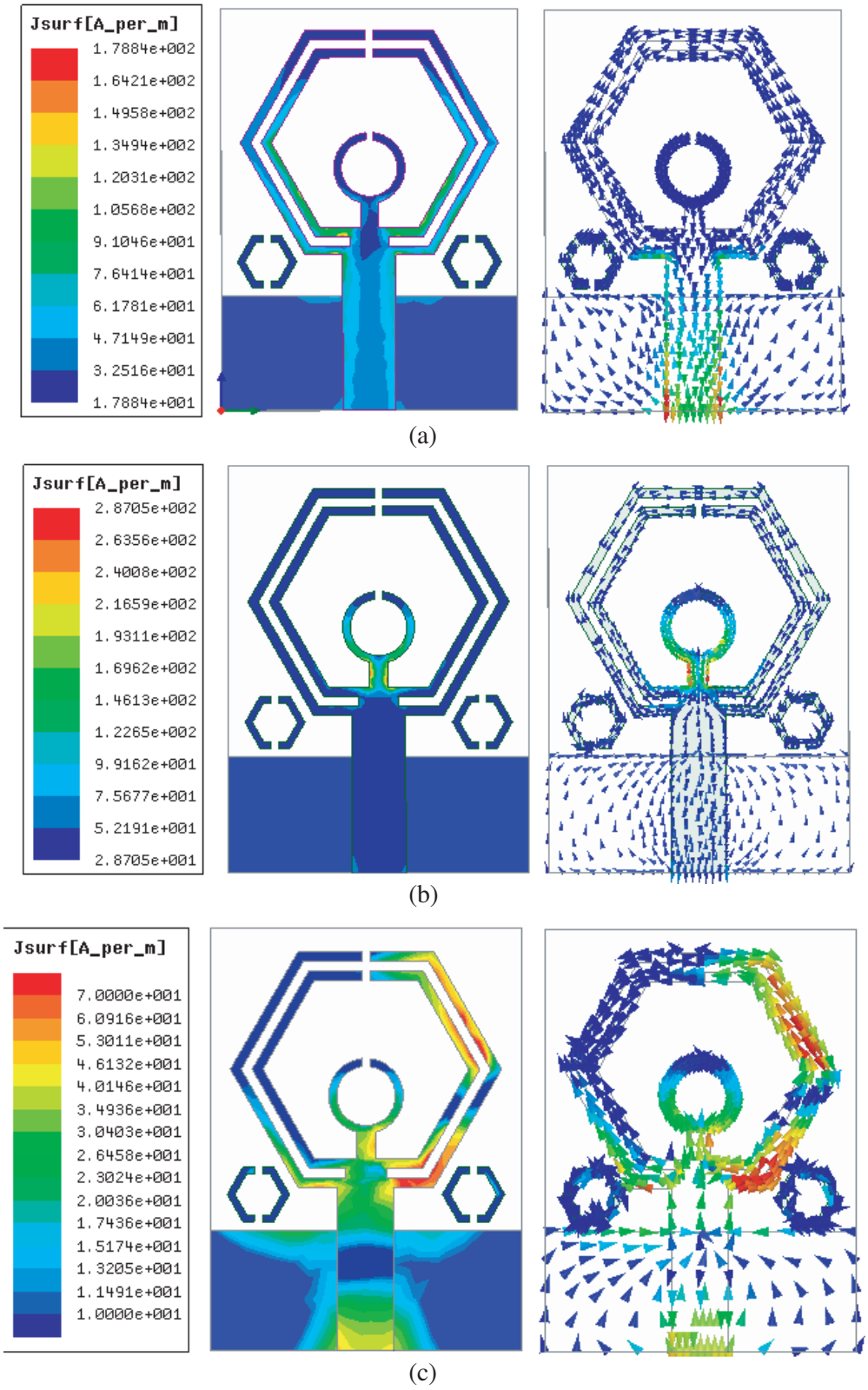

Figure 15. Simulated surface and vector current distribution of the proposed antenna. (a) At 3.5 GHz. (b) At 5.05 GHz. (c) At 6.2 GHz.

Table 2. Comparison between the proposed antenna with existing antenna.

Ref. No.	Concept	Metamaterial Functions	Antenna Volume (mm^3)	No. of bands	Frequency (GHz)	Impedance Bandwidth (%)	Measured Gain (dB)	Efficiency (%)
[13]	Triangular SRR	Multiband	768	2	2.40–2.48, 4.70–6.04	3.26, 4.56	2.28, 1.96	62.53, 93.25
[29]	Circular SRR	Multiband	2560	2	1.00–3.00, 3.20–11.00	-	6.00	70.00
[30]	Circular CSRR	Wide band	1000	1	4.49–21.85	-	1.05, 6.03	64.80, 92.52
[34]	Eight shaped metamaterial SRR	Gain enhancement	160200	1	7.18–8.44	16.10	14.00	-
[35]	Circular SRR	Gain enhancement	180000	1	3.2–4.9	41.90	8.00	-
[36]	Rectangular SRR	Gain enhancement and Wide band	326095	1	9.7–12.3	26.80	11.90	78.00
Proposed Work	HSRR-CSRR and D-HSRR	Multiband and Bandwidth enhancement	864	2	3.42–3.85, 4.82–6.85	11.82, 34.79	1.7, 1.6, 1.8	97.00, 91.23, 90.84

the width of the two concentric hexagonal rings.

A comparative analysis of different parameters such as physical size, number of operating bands, percentage impedance bandwidth, gain, and efficiency of the designed antenna is done concerning the previous literature and is illustrated in Table 2. It is apparent from Table 2 that the proposed antenna provides bandwidth by keeping the antenna's size small, with comparative gain and efficiency with that of the existing antenna design. Also, it is simple in design for easy fabrication.

6. CONCLUSION

The proposed novel miniaturized HSRR-CSRR inspired printed antenna is designed, fabricated, and tested. The size reduction of 51.23% is achieved using the HSRR-CSRR metamaterial structure. The negative parameter of the HSRR-CSRR metamaterial structure has been investigated and verified from the permeability graph. A D-SHSRR structure has been used for bandwidth enhancement. The proposed antenna's measured reflection coefficient (dB) results have shown good agreement with the simulated ones. The antenna's measured impedance bandwidths are about 625 MHz in the first band of 3.225 GHz–3.850 GHz and 2030 MHz in the second band of 4.82 GHz–6.85 GHz. The proposed antenna has the measured maximum gains of 1.7 dB, 1.6 dB, and 1.8 dB at 3.5 GHz, 5.05 GHz, and 6.2 GHz, respectively, and maximum efficiency of about 90%. This antenna meets the requirements of upcoming Sub-6 GHz 5G NR and IEEE 802.11ba/be (Wi-Fi) applications.

REFERENCES

1. Marcus, M. J., "5G and 'IMT for 2020 and beyond' [spectrum policy and regulatory issues]," *IEEE Wireless Communication*, Vol. 22, No. 4, 2–3, Aug. 2015.

2. "IEEE P802.11 Task Group BA — Wake-up Radio Operation," www.ieee802.org, retrieved Aug. 12, 2020.
3. Shankland, S., "Wi-Fi 6 is barely here, but Wi-Fi 7 is already on the way — With improvements to Wi-Fi 6 and its successor, Qualcomm is working to boost speeds and overcome congestion on wireless networks," *CNET*, Retrieved Aug. 20, 2020.
4. Caloz, C. and T. Itoh, *Electromagnetic Metamaterials: Transmission Line Theory and Microwave Applications*, 1st Edition, Wiley-IEEE Press, Hoboken, NJ, ISBN-10: 0471669857, 2006.
5. Marque's, R., F. Martin, and M. Sorolla, *Metamaterials with Negative Parameters: Theory, Design and Microwave Applications*, Wiley, Hoboken, NJ, ISBN: 978-0-471-74582-2, 2007.
6. Gunavathi, N. and D. Sriram Kumar, "Miniaturized unilateral coplanar waveguide-fed asymmetric planar antenna with reduced radiation hazards for 802.11ac application," *Microwave and Optical Technology Letters*, Vol. 58, No. 2, 337–342, 2016.
7. Gunavathi, N. and D. Sriram Kumar, "CPW-fed monopole antenna with reduced radiation hazards towards human head using metallic thin-wire mesh for 802.11ac application," *Microwave and Optical Technology Letters*, Vol. 57, No. 11, 2684–2687, 2015.
8. Gunavathi, N. and D. Sriram Kumar, "Estimation of resonant frequency and bandwidth of compact unilateral coplanar waveguide-fed flag shaped monopole antennas using artificial neural network," *Microwave and Optical Technology Letters*, Vol. 57, No. 2, 337–342, 2015.
9. Hu, J. R. and J. S. Li, "Compact microstrip antennas using CSRR structure ground plane," *Microwave and Optical Technology Letters*, Vol. 56, No. 1, 117–120, 2014.
10. Chaturvedi, D. and S. Raghavan, "A compact metamaterial inspired antenna for WBAN applications," *Wireless Personal Communications*, Vol. 105, 1449–1460, 2019.
11. Imaculate Rosaline, S. and S. Raghavan, "Metamaterial inspired split ring monopole antenna for WLAN applications," *ACES Express Journal*, Vol. 1, No. 5, 2016.
12. Rajalakshmi, P. and N. Gunavathi, "Gain enhancement of cross-shaped patch antenna for IEEE 802.11ax Wi-Fi applications," *Progress In Electromagnetics Research Letters*, Vol. 80, 91–99, 2018.
13. Garg, P. and P. Jain, "Design and analysis of a metamaterial inspired dual-band antenna for WLAN applications," *International Journal of Microwave and Wireless Technologies*, 2019.
14. Samson Daniel, R., R. Pandeeswari, and S. Raghavan, "A Compact metamaterial loaded monopole antenna with offset-fed microstrip line for wireless applications," *International Journal of Electronics and Communication (AEU)*, Vol. 83, 88–94, 2018.
15. Wu, K., Y. Huang, R. Wen, J. Li, and G. Wen, "Comparison analysis of single loop resonator-based miniaturized triple-band planar monopole antennas," *International Journal of Antennas and Propagation*, 2015.
16. Lajevardi, M. E. and M. Kamyab, "Ultra miniaturized metamaterial — Inspired SIW textile antenna for off-body applications," *IEEE Antenna and Wireless Propagation Letters*, Vol. 16, 3155–3158, 2017.
17. Si, L. M., Q. L. Zhang, W. D. Hu, W. H. Yu, et al., "A uniplanar triple-band dipole antenna using complementary capacitively-loaded loop," *IEEE Antennas and Wireless Propagation Letters*, Vol. 14, 743–746, 2015.
18. Li, K., C. Zhu, L. Li, Y. M. Cai, and C. H. Liang, "Design of electrically small metamaterial antenna with ELC and EBG loading," *IEEE Antennas and Wireless Propagation Letters*, Vol. 12, 678–681, 2013.
19. Ameen, M. and R. K. Chaudhary, "Dual-layer and dual-polarized metamaterial inspired antenna using circular — Complementary split ring resonator mushroom and metasurface for wireless applications," *International Journal of Electronics and Communication (AEU)*, Vol. 113, 152977, 2019.
20. Rajalakshmi, P. and N. Gunavathi, "Compact complementary folded triangle split ring resonator triband mobile handset planar antenna for voice and Wi-Fi applications," *Progress In Electromagnetics Research C*, Vol. 91, 253–264, 2019.

21. Rajalakshmi, P. and N. Gunavathi, "Compact modified hexagonal spiral resonator-based tri-band patch antenna with octagonal slot for Wi-Fi/WLAN applications," *Progress In Electromagnetics Research C*, Vol. 106, 77–87, 2020.
22. Rajabloo, H., V. A. Kooshki, and H. Oraizi, "Compact microstrip fractal Koch slot antenna with ELC coupling load for triple band applications," *International Journal of Electronics and Communication (AEU)*, Vol. 73, 144–149, 2017.
23. Si, L.-M. and X. Lv, "CPW-fed multiband omnidirectional planar microstrip antenna using metamaterial resonators for wireless communications," *Progress In Electromagnetic Research*, Vol. 83, 133–146, 2008.
24. Xi, L., H. Zhai, and L. Li, "A compact low profile dual-polarized filtering antenna with metamaterial for wide-band base station applications," *Microwave and Optical Technology Letters*, Vol. 60, 64–69, 2017.
25. Dong, Y., H. Toyao, and T. Itoh, "Compact circularly-polarized patch antenna loaded with metamaterial structures," *IEEE Transactions on Antenna and Propagation*, Vol. 59, No. 11, 4329–4333, 2011.
26. Nasimuddin, N., Z. N. Chen, and X. Qing, "Bandwidth enhancement of a single-feed circularly polarized antenna using a metasurface: Metamaterial-based wide-band circularly polarized rectangular microstrip antenna," *IEEE Antennas and Propagation Magazine*, Vol. 58, No. 2, 39–46, 2016.
27. Joshi, A. and R. Singhal, "Probe-fed wide-band AMC-integrated hexagonal antenna with uniform gain characteristics for WLAN applications," *Wireless Networks*, 2020.
28. Gong, X., L. Tong, and Y. Tian, "Design of a microstrip-fed hexagonal Shape UWB antenna with triple band-notched bands," *Progress In Electromagnetic Research C*, Vol. 62, 77–87, 2016.
29. Heydari, S., K. Pedram, Z. Ahmed, and F. B. Zarrabi, "Dual-band monopole antenna based on metamaterial structure with narrowband and UWB resonances with reconfigurable quality," *AEU — International Journal of Electronics and Communications*, Vol. 81, 92–98, 2017.
30. Islam, S. S., T. Alam, M. R. Iqbal Faruque, and M. T. Islam, "Design and analysis of a Complementary Split-Ring Resonator (CSRR) metamaterial-based antenna for wide-band application," *Science and Engineering of Composite Materials*, Vol. 24, No. 5, 2015.
31. Yves, S., T. Berthelot, M. Fink, G. Lerosey, and F. Lemoult, "Left-handed band in an electromagnetic metamaterial induced by subwavelength multiple scattering," *Appl. Phys. Lett.*, Vol. 111101, Mar. 2018.
32. Chen, H., J. J. Zhang, Y. Bai, Y. Luo, and L. Ran, "Experimental retrieval of the effective parameters of metamaterial based on a waveguide method," *Optics Express*, Vol. 14, No. 26, 2006.
33. Smith, D. R., S. Schultz, P. Markos, and C. M. Soukoulis, "Determination of negative permittivity and permeability of metamaterials from reflection and transmission coefficients," *Phys. Rev. B*, 2002.
34. Pandey, A. K., M. Chauhan, V. K. Killamsety, and B. Mukherjee, "High gain compact rectangular dielectric resonator antenna using metamaterial as superstrate," *International Journal of RF and Microwave Computer-Aided Engineering*, Vol. 29, No. 12, 1–10, Wiley, 2019.
35. Sinha, M., V. Killamsetty and B. Mukherjee, "Near field analysis of RDRA loaded with split ring resonators superstrate," *Microwave and Optical Technology Letters*, Vol. 60, No. 2, 472–478, Wiley, 2018.
36. Chauhan, M., A. Rajput, and B. Mukherjee, "Wideband circularly polarized low profile dielectric resonator antenna with meta superstrate for high gain," *AEU — International Journal of Electronics and Communication*, 128, 2021.